Facile Synthesis of Surfactant-Free Au Cluster/Graphene Hybrids for High-Performance Oxygen Reduction Reaction

Huajie Yin,[†] Hongjie Tang,[†,‡] Dan Wang,[‡] Yan Gao,[†,*] and Zhiyong Tang[†,*]

[†]Laboratory of Nanomaterials, National Center for Nanoscience and Technology, Beijing, 100190, People's Republic of China and [‡]State Key Laboratory of Multiphase Complex Systems, Institute of Process Engineering, Chinese Academy of Sciences, Beijing, 100190, People's Republic of China

Fuel cells are expected to become a reliable source of clean energy with broad applications in both electric vehicles and portable electronics, because they provide a direct way to convert chemical energy to electricity without combustion and can easily achieve high efficiencies in energy conversion terms.[1−4] Currently, a major limiting factor for the practical application of fuel cells is the sluggish kinetics of the oxygen reduction reaction (ORR) at the cathode, which gives rise to the larger overpotential and lower current density. Generally, platinum (Pt) and Pt alloys are the most active catalysts for ORR; however, they still suffer from serious durability and reliability problems including the crossover and poisoning effects.[2−4] Besides, the scarcity and cost of Pt, together with the aforementioned limits, have hampered the large-scale application of fuel cells. It is therefore of importance to explore new strategies, including (1) decrease of the use amount of Pt and (2) development of the non-Pt electrocatalysts, to address these problems lying in both fundamental research and applied technology.[5−9]

Bulk gold (Au) and other non-Pt metals have attracted little attention in electrocatalysis toward ORR due to their poor catalytic performance that is confirmed by both experimental evidence and density functional theory (DFT) calculations.[3,10] Fortunately, recent studies have demonstrated that the Au particles with the sizes of less than 2 nm, which are also known as clusters differentiating from nanoparticles (NPs) due to their small sizes and narrow size distribution,[11] have much higher electrocatalytic activity for ORR than the bulk Au and larger Au NPs.[12,13] The enhanced catalytic activity of Au clusters is accounted for by the high fraction of low-coordinated surface atoms and that oxygen molecules can be

ABSTRACT Non-Pt noble metal clusters like Au clusters are believed to be promising high performance catalysts for the oxygen reduction reaction (ORR) at the cathode of fuel cells, but they still suffer big problems during the catalysis reactions, such as a large amount of the capping agents being on the surface and easy occurrence of dissolution and aggregation. To overcome these obstacles, here, we present

a novel and general strategy to grow ultrafine Au clusters and other metal (Pt, Pd) clusters on the reduced graphene oxide (rGO) sheets without any additional protecting molecule or reductant. Compared with the currently generally adopted nanocatalysts, including commercial Pt/C, rGO sheets, Au nanoparticle/rGO hybrids, and thiol-capped Au clusters of the same sizes, the as-synthesized Au cluster/rGO hybrids display an impressive eletrocatalytic performance toward ORR, for instance, high onset potential, superior methanol tolerance, and excellent stability.
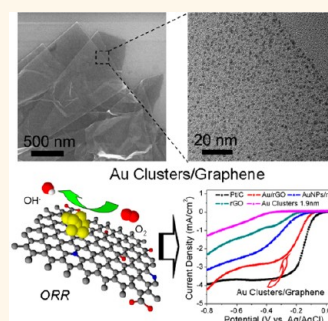
adsorbed on the cluster surface and activated more easily than the close-packed counterparts.[12−17] The utilization of the clusters as the electrocatalysts will not only dramatically improve the efficiency of ORR but also considerably decrease the materials cost.

However, Au clusters used alone are frequently subject to two main disadvantages in the electrocatalytic reactions. First, the capping agents on the surface of the clusters may block the mass transport and electron transfer, which seriously impair their electroactivity.[18,19] Second, owing to the extremely small size and high surface energy, the durability of metal clusters is largely restricted by the easy occurrence of dissolution, aggregation, and sintering during catalysis reactions.[13] To overcome these obstacles, a plausible solution is to anchor Au clusters on the specific supports with less or

* Address correspondence to
zytang@nanoctr.cn,
gaoyan@nanoctr.cn.

even without capping agents.[20] Among all the available support materials, graphene, as a robust two-dimensional sheet of sp^2-hybridized carbon, has emerged as the most promising one.[21−23] The combination of its high surface area, enhanced mobility of charge carriers, and good stability makes graphene an ideal platform for growing or anchoring functional nanomaterials, such as metal and semiconductor NPs.[24−28] Theoretical calculations have predicted that the metal clusters supported on graphene would generate excellent catalytic activity by the increased charge transfer from the clusters to the substrates, while their stability could be obviously improved through hybridization between the clusters and sp^2 dangling bonds at the defect sites of graphene.[29−31] Though much progress has been made on the synthesis and electrochemical property investigation of NP/graphene hybrids, the corresponding study on metal cluster/graphene hybrids is rarely reported. Compared with that of NPs, synthesis of the small sized clusters with narrow size distribution on graphene represents many more challenges because of its high requirement of control over the nucleation and growth processes. Furthermore, the capping agents, which are typically used for tuning the growth of metal clusters in the solution, are not easily compatible with graphene and possibly cause deleterious influences on the metal/graphene interfaces.

Herein, we present a novel and simple strategy, which is called the "clean" method, to grow Au and other metal (Pt, Pd) clusters on the reduced graphene oxide (rGO) sheets in the absence of any additional protecting molecule or reductant. The strong absorption and the moderate reduction of rGO sheets toward metal ions in the solution are the key for providing the initial nuclear sites and restraining the growth of Au clusters. The synthesized Au cluster/rGO (Au/rGO) hybrids exhibit the extraordinary activity toward ORR.

RESULTS AND DISCUSSION

Well-dispersed rGO sheets in an alkaline solution (ammonia, pH = 11) were synthesized by following the established recipe with a minor modification,[32] and the as-prepared solution containing 0.17 mg/mL graphene sheets was set aside for at least two weeks to remove the residual N_2H_4. In a typical preparation of Au/rGO hybrids, 100 μL of 50 mM $HAuCl_4$ solution was added to 10 mL of rGO solution at room temperature with sonication, and subsequently the mixture was allowed to stand for 10 min. The suspensions were collected by centrifugation and thoroughly washed with pure water. Finally, Au/rGO products were obtained by the freeze-drying process.

Several important features of the synthesized Au/rGO hybrids can be discerned upon the microscopic and spectroscopic characterization: (1) A large-scale scanning electron microscopy (SEM) image (Figure 1A) confirms that the products remain in the shape of the flexible two-dimensional sheets, and no evident phase separation is found. (2) The close observation of the transmission electron microscopy (TEM) images (Figure 1B−D and Supporting Information, Figure S1) further reveals that Au clusters with monodisperse sizes are homogenously dispersed on the surface of rGO sheets, and no free cluster is formed outside the rGO sheets. (3) The size distribution of Au clusters estimated from the high angle annular dark field image has a typical Gaussian shape, where the average diameter of Au clusters is 1.8 nm with a narrow dispersion of 0.2 nm (inset in Figure 1D). (4) On the basis of the similarity in Raman spectra of Au/rGO hybrids and pure rGO sheets, it is concluded that the formation of Au clusters does not greatly reduce the sizes of in-plane sp^2 domains of graphene.[33] One reasonable explanation is that the content of Au in the hybrids is 1.8 atom % (estimated from Figure 1F), which is not enough to cause large structural damage of rGO sheets. (5) Last but not least, the X-ray photoelectron spectroscopy (XPS) signature of Au 4f doublet ($4f_{7/2}$ and $4f_{5/2}$) is deconvoluted into two pairs of peaks, corresponding to the reduced Au(0) clusters and the Au(III) ions, respectively (inset in Figure 1F). Considering the electrostatic balance, the presence of positively charged Au(III) ions suggests that there should be a dynamic electron transfer from the Au clusters to the underlying rGO in the Au/rGO hybrids, leading to net negative charges of the rGO. Such an electron transfer from the nanoparticles to graphene is recently confirmed by both theoretical calculation and experimental observation.[30] Furthermore, there is a 1 eV red shift of XPS peak of Au(0) clusters (84.8 eV) compared with bulk Au (83.8 eV).[34,35] This shift in the binding energy is typical for very small metal NPs on a variety of support materials, and is generally attributed to reduced core-hole screening in metal clusters. This result highlights that the electronic properties of the Au clusters are significantly different from bulk materials and bigger Au NPs,[34,35] and such size-dependent alteration of electronic structures likely leads to the unusual electrocatalytic properties.

Furthermore, the products synthesized under other conditions were also investigated for a better understanding of this "clean" preparation method. First, the sizes of the synthesized clusters are easily tuned by altering the reaction time, and prolonging the reaction time leads to the gradual size growth of Au clusters. Interestingly, the density (2.8 ± 0.7 particles/100 nm^2) and the size distribution (less than 20%) of Au clusters remain almost intact with increasing size (Supporting Information, Figure S2), indicating that an instantaneous heteronucleation process occurs and no obvious Ostwald ripening takes place in the subsequent growth. This phenomenon suggests that (1) a strong anchoring effect exists between Au clusters and the rGO surface,[36] and (2) there are enough Au ion precursors to preserve the size focusing during the cluster growth (inset in Figure 1F). Second, change of the reaction temperature
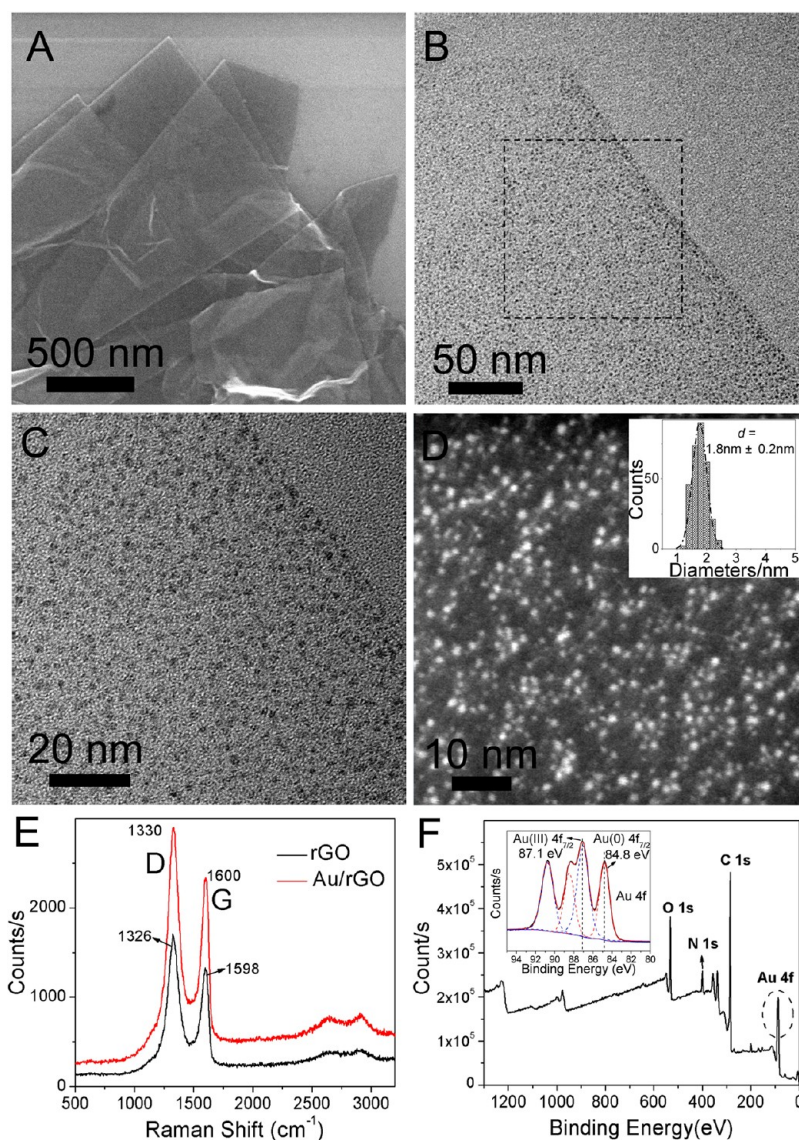
Figure 1. (A) SEM image, (B,C) TEM, (D) HAADF, (E) Raman spectrum, and (F) XPS spectrum of as-synthesized Au/rGO hybrids. Inset in panel D stands for the statistic histogram of Au cluster sizes, while inset in panel F represents the XPS spectrum of Au element in Au/rGO hybrids.

only has slight influence on the sizes of products (Supporting Information, Figure S2). For example, the size of Au clusters grows up to 3.2 nm at 90 °C after a 2 h reaction, while the diameter of Au clusters reacted at room temperature is around 2.5 nm after 2 h. Regardless of the reaction temperature, all the Au cluster products have the narrow size distribution, further demonstrating that the anchoring ability of rGO sheets keeps strong even at high temperature. Third, the reduction capability of rGO sheets is found to play an important role on the sizes of the Au particles (Supporting Information, Figure S3). The reduction capability of rGO sheets can be altered by adding various amounts of N_2H_4 (see the Supporting Information experimental section and Figure S3), and the Au/rGO hybrids are only obtained with the rGO sheets of a proper reduction level. Bigger Au NPs attached on the rGO surface are the main products

in the presence of rGO sheets with either insufficient or excessive reduction.

What is the possible mechanism for Au clusters grown on the rGO surface by this "clean" method? To answer this question, we carried out another series of experiments combined with XPS characterization. Au/rGO hybrids are synthesized with varying concentration of $HAuCl_4$ from 0.5 and 1 mM to 2 mM, and the corresponding products are named as Au/rGO-1, Au/rGO-2, and Au/rGO-3, respectively. From their XPS spectra shown in Supporting Information, Figures S4 and S5, the Au content in these hybrids is estimated to be 1.8 atom % (Au/rGO-1), 3.1 atom % (Au/rGO-2) and 7.2 atom % (Au/rGO-3), respectively. This result is in accordance with the TEM analysis (Supporting Information, Figure S6), in which the intensity of Au clusters on the graphene substrates increases as the concentration of Au
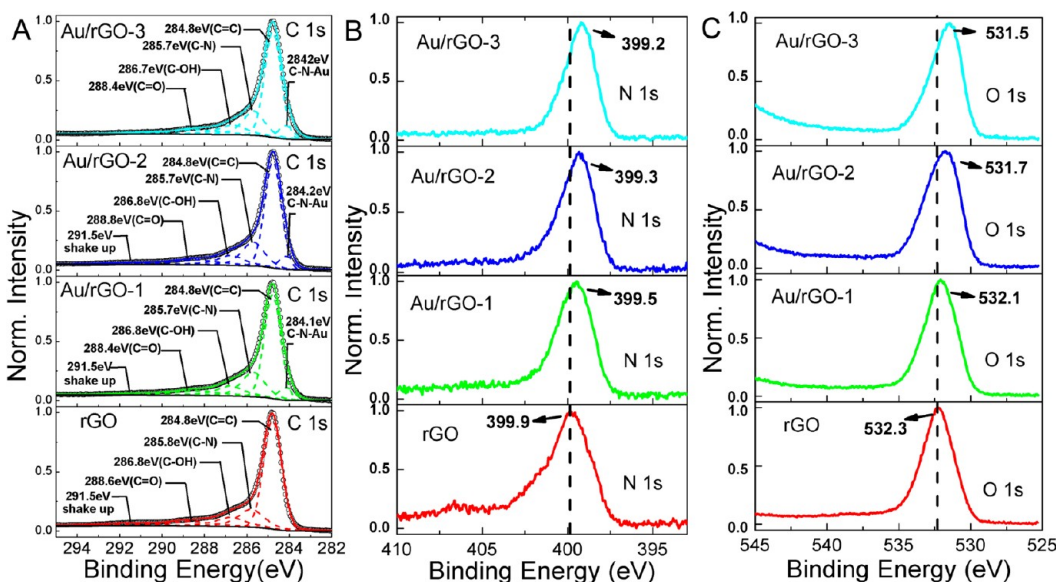
Figure 2. (A−C) XPS spectra of the C 1s region, N 1s region, O 1s region of rGO, Au/rGO-1, Au/rGO-2, and Au/rGO-3, respectively. Synthesis conditions: Au/rGO-1 (0.5 mM HAuCl₄), Au/rGO-2 (1 mM HAuCl₄), Au/rGO-3 (2 mM HAuCl₄) in 0.17 mg/mL rGO solution; room temperature; 1 h.

precursors (HAuCl₄) increases. The high-resolution C 1s XPS spectrum of rGO (Figure 2A) can be fitted into four peaks, corresponding to C atoms in different functional groups: the nonoxygenated ring C at 284.8 eV, the C bound to nitrogen at 285.8 eV, the C in C−O bonds at 286.8 eV and the carbonyl C at 288.4 eV.[37−39] This XPS result reveals that there are numerous defects containing heteroatoms on the rGO plane and edges.[39] By introducing Au clusters after the reaction, an additional peak at 284.1 eV appears, which is attributed to the C−N−Au bond.[40] Moreover, from Figure 2B,C, one can see that there is a blue shift of the binding energy of N 1s and O 1s, and the shift amplitude is proportional to the content of Au clusters. The blue shift of XPS peaks demonstrates that the Au/rGO is a covalent hybrid based on the coordination or chemical effects between the heteroatoms, for example, N and O, and Au clusters.[41−43] It should be noted that such covalent hybridization would considerably reduce the migration and fusion of Au clusters on the graphene substrates, resulting in the significant improvement of the stability of Au clusters in the electrocatalytic reaction.

Scheme 1 illustrates the formation mechanism of Au/rGO hybrids. First of all, the *in situ* generated rGO sheets are highly negative-charged with a zeta potential ranging from −45 to −50 mV as measured experimentally. When metal ions are added to the rGO solution, rGO sheets exhibit high absorption capacity toward positive-charged Au(III) ions *via* partial replacement of Cl⁻ ligands,[44,45] which are confirmed by the decreased zeta potential (after adding Au ions, the zeta potential is found to be reduced from *ca.* −50 to *ca.* −10 mV). Second, most Au(III) ions will coordinate with the heteroatoms at the defects on the rGO sheets, especially for N atoms, which act as the initial nucleation

site for Au clusters. Very recently, DFT investigation disclosed that the Au subnanoclusters would be nucleated and grown at the defects of the rGO sheets, particularly on N-induced defects.[37] The calculation results show that the binding energy of a Au atom for filling a carbon divacancy site is about 3.40 eV, which is larger than the cohesive energy of the face-centered cubic Au (3.1 eV). So the divacancy could be a nucleation site for the growth of Au subnanoclusters. Third, rGO sheets are the electron donors or the reductants for subsequent Au cluster growth on the rGO surface. Previous reports have explored that both single-wall carbon nanotubes (SWNTs)[46] and graphene oxide sheets[36] could, respectively, reduce AuCl₄³⁻ and PdCl₄²⁻ to generate Au NPs and Pd NPs without any additional reductant. These phenomena are explained by the difference in the redox potentials of AuCl₄³⁻ ions and SWNTs (0.5 V *vs* SCE) or PdCl₄²⁻ and graphene oxide (0.48 V *vs* SCE), which facilitates the reduction of noble metal ions. Similar to these carbon materials, rGO sheets are also good reducing agents for the formation of Au/rGO nanocomposites.

It needs to be pointed out that the selective absorption and the restricted deposition of metal ions on the rGO sheet are the prerequisite condition for generating the metal cluster/rGO hybrids. Only the rGO sheets, which have the moderate number of the heteronuclear sites as well as the moderate reducing capability, give rise to the production of Au/rGO hybrids.[47,48] The rGO sheets formed *via* the insufficient reduction would have many defects that act as the excessive nucleation sites, increase the possibility of aggregation and fusion between the adjacent Au clusters, and result in the generation of bigger NPs (Supporting Information, Figure S3). On the contrary, there
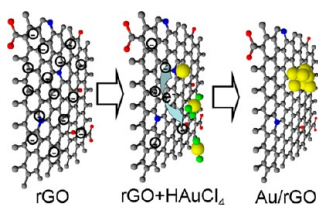
Scheme 1. Scheme of the Formation Mechanism of Au/rGO Hybrids: C (black ball), N (blue ball), O (red ball), H (white ball), Au (golden ball), Cl (green ball)

are much less nucleation sites on the rGO surfaces of strong reduction ability, but the growth rate of Au clusters is largely enhanced, leading to production of the NPs with large sizes (Supporting Information, Figure S3).

On the basis of the above understanding of the formation mechanism, a couple of other hybrid systems have been tried. The Pd cluster/rGO hybrids were successfully synthesized by mixing rGO sheets with $PdCl_4^{2-}$, and the average diameter of Pd clusters is about 1.4 nm (Figure 3A–C). For production of Pt cluster/rGO hybrids, a two-step method is adopted. Different from direct reduction of $AuCl_4^{3-}$ and $PdCl_4^{2-}$ into elementary Au and Pd, the reduction of $PtCl_6^{4-}$ undergoes a two-step process, from $PtCl_6^{4-}$ to $PtCl_4^{2-}$ to Pt.[49] Furthermore, the reduction potential of reaction, $PtCl_4^{2-} + 2e^- \rightarrow Pt^{2+}$, is +0.72 V, which is lower than that of $AuCl_4^{3-}$ ($AuCl_4^{3-} + 3e^- \rightarrow Au$, $E^\ominus = +1.02$ V) and $PdCl_4^{2-}$ ($PdCl_4^{2-} + 2e^- \rightarrow Pd$, $E^\ominus = +0.83$ V).[49] As a result, the rGO sheets can only partially reduce Pt^{4+} to Pt^{2+} (Supporting Information, Figure S7). By slowly adding $NaBH_4$ solution, the Pt clusters with the average diameter of 1.9 nm are formed on the rGO surface (Figure 3D–F). Evidently, the "clean" method will be a novel and general strategy to fabricate different types of metal/rGO hybrids.

The ORR electrocatalytic activity of the prepared Au/rGO hybrids is evaluated by cyclic voltammetry (CV) scanning in O_2 or N_2 saturated 0.1 M KOH aqueous solutions at room temperature (Figure 4A). The comparison of the three CV curves in Figure 4A clearly shows the exceptional ORR catalytic activity of Au/rGO. Similar to the commercial Pt/C (Figure 4B), a characteristic ORR peak appears in the O_2-saturated KOH solution for Au/rGO hybrids. The ORR onset potential is at *ca.* −0.08 V (*vs* Ag/AgCl) with a reduction peak at *ca.* −0.19 V (*vs* Ag/AgCl), which are close to those of commercial Pt/C catalyst (Figure 4B) and superior than the reported Au clusters and Au/carbon hybrid catalysts,[12,13,50−53] displaying the remarkable catalytic performance of Au/rGO hybrids for ORR. To test the tolerance of Au/rGO hybrids to methanol fuel, CV in the O_2-saturated 0.1 M KOH solution containing 3 M methanol is recorded. No noticeable change is observed for Au/rGO electrode (blue curve in Figure 4A), whereas the cathodic peak for oxygen reduction almost disappears at the commercial Pt/C electrode coupled with one pair of peaks characteristic of methanol

reduction/oxidation. These results demonstrate that, different from the commercial Pt/C, the Au/rGO hybrids possess high selectivity for ORR with great tolerance to possible crossover effects, which is critical for applications in the direct methanol alkaline fuel cells.

Linear-sweep voltammetry (LSV) curves of oxygen reduction for Au/rGO in an O_2-saturated 0.1 M KOH solution are recorded at a rotating disk electrode (RDE) at different rotation rates (ω) from 225 to 3600 rpm (Figure 4C). At 1600 rpm, the Au/rGO electrode exhibits an ORR onset potential of about −0.10 V (*vs* Ag/AgCl), and the corresponding ORR current density (J) reaches around 4.1 mA/cm² at −0.8 V (*vs* Ag/AgCl). The Koutecky−Levich plots (J^{-1} *vs* $\omega^{1/2}$) at various electrode potentials (from −0.3 to −0.7 V *vs* Ag/AgCl) are presented in the inset of Figure 4C. The transferred electron number (n) per oxygen molecule for Au/rGO is derived to be 3.7−3.9 over the potential range from −0.3 to −0.7 V *vs* Ag/AgCl according to the *K−L* equation. The rotating ring-disk electrode (RRDE) measurement (Figure 4D) further proves that there is negligible ring current, and *n*, calculated from RRDE curves in the inset of Figure 4D, is about 3.6−3.7 over the potential range from −0.3 to −0.7 V *vs* Ag/AgCl. Both of the experimental results demonstrate that the four-electron process is the dominating pathway for the oxygen reduction on the Au/rGO electrode, which will benefit the construction of fuel cells with high efficiency.[2,3]

The electrocatalytic activities of the currently generally adopted nanocatalysts, including commercial Pt/C, rGO sheets, Au NP/rGO hybrids (Au NP/rGO), and thiol-capped Au clusters of the same size, are compared with Au/rGO hybrids by recording the corresponding RDE curves (1600 rpm) for ORR (Figure 5A). The synthesis of Au NP/rGO and Au clusters is described in the Supporting Information, and Figure S8 shows that the average diameters of the obtained Au NPs and Au clusters are ∼7.0 nm and ∼1.9 nm, respectively. From Figure 5A, it is clear the ORR onset potential of Au/rGO hybrids (−0.10 V) is more positive than that of Au NP/rGO hybrids (−0.20 V), rGO sheets (−0.22 V), and thiol-capped Au clusters (−0.32 V). Furthermore, the ORR current density (*e.g.*, at −0.8 V *vs* Ag/AgCl) of Au/rGO hybrids (4.11 mA/cm²) is also much higher than those of Au NP/rGO hybrids (2.96 mA/cm²), rGO sheets (2.14 mA/cm²), and thiol-capped Au clusters (1.27 mA/cm²). The possible reason for the superior ORR activity of Au/rGO hybrids should be ascribed to three main factors: First, the small size effects of Au clusters benefit activating oxygen molecules (Au/rGO hybrids *vs* Au NP/rGO hybrids). The decreased coordination of Au together with the reduced electrophilicity of the small clusters give rise to a corresponding decrease in the activation energy of the dissociative chemisorption of molecular O_2, which further facilitates the 4-electron reduction of molecular O_2 and thus leads to a positive onset potential.[12,13,53,54] Second, the absence of the capping molecules and
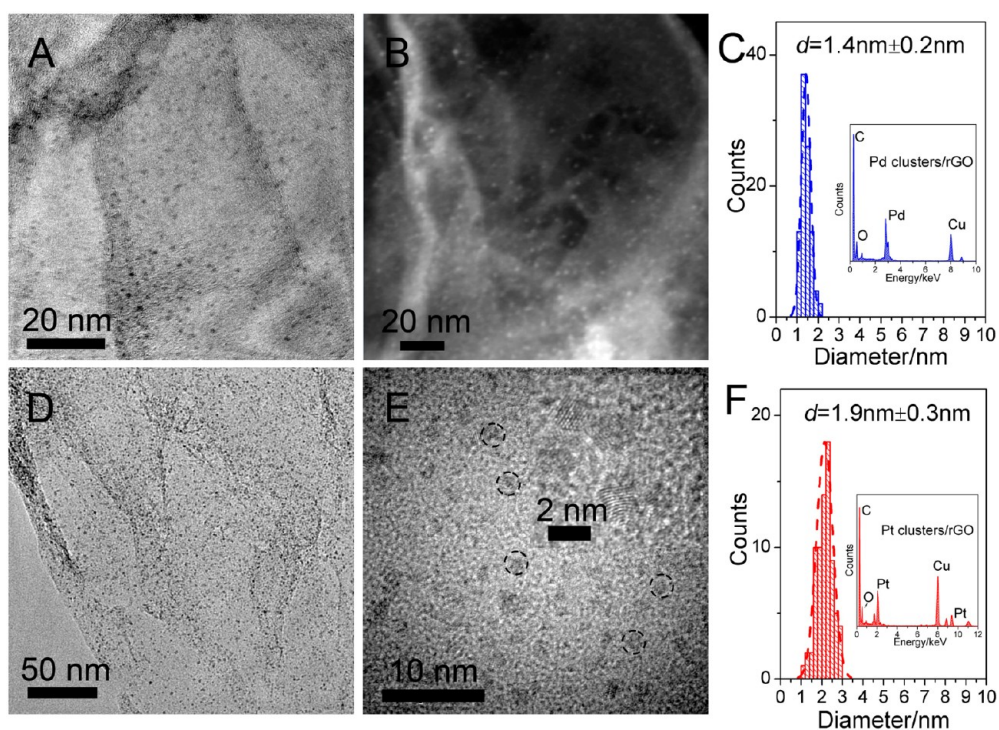
Figure 3. (A) TEM and (B) HAADF image of Pd cluster/rGO hybrids, (C) the statistic histogram of Pd cluster sizes; the inset represents energy-dispersive X-ray (EDX) spectrum of Pd cluster/rGO hybrids, (D, E) TEM images of Pt cluster/rGO hybrids, (F) the statistic histogram of Pt cluster sizes; the inset represents EDX spectrum of Pt cluster/rGO hybrids.
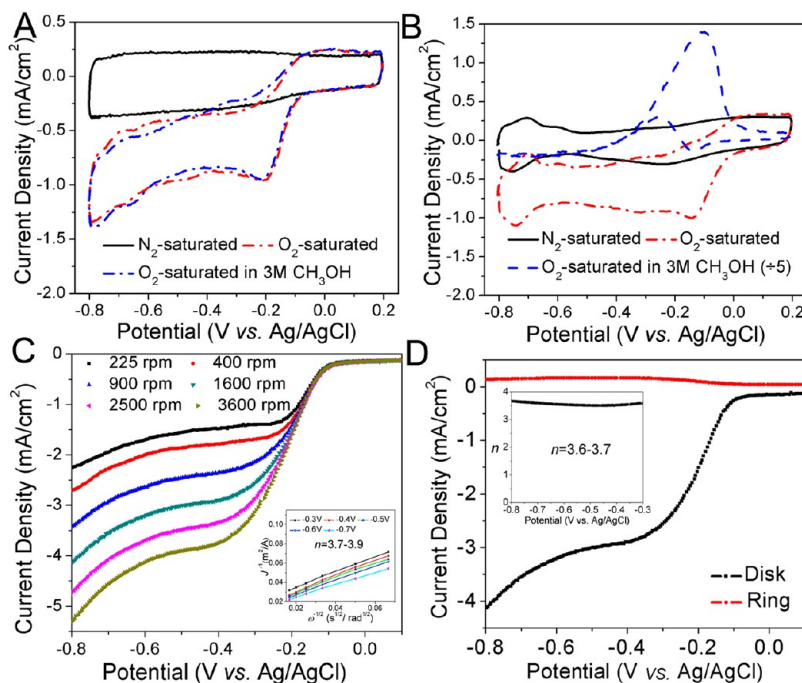

Figure 4. CV curves of (A) Au/rGO hybrids and (B) commercial Pt/C (20 wt %) on a glass carbon electrode in N_2-saturated 0.1 M KOH (black curves), O_2-saturated 0.1 M KOH (red curves), and O_2-saturated 3 M CH_3OH solutions (blue curves). (C) Rotating disk electrode (RDE) curves of Au/rGO hybrids in O_2-saturated 0.1 M KOH at different speeds. Inset presents the Koutecky–Levich plots derived from the RDE measurements. (D) Rotating ring-disk electrode (RRDE) curves of Au/rGO hybrids in O_2-saturated 0.1 M KOH at 1600 rpm. The disk potential was constant at 0.5 V vs Ag/AgCl. All the scanning rates were 50 mV/s.

proper gold loading in the hybrids promote the efficient interfacial charge transfer during the ORR reactions (Au/rGO hybrids vs Au clusters).[18,19,55] Third, the combination of Au clusters and rGO provides a synergetic coupling effect for the enhanced ORR activity (Au/rGO hybrids vs rGO sheets and Au clusters). Graphene in
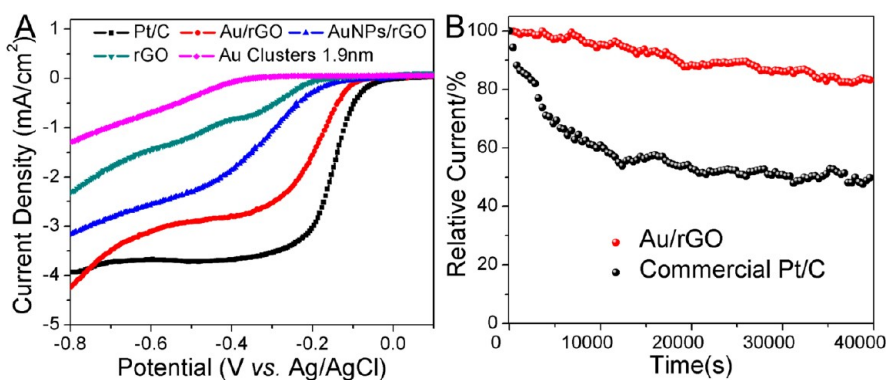
Figure 5. (A) RDE curves of commercial Pt/C, Au/rGO hybrids, Au NP/rGO hybrids, rGO sheets, Au clusters in O_2-saturated 0.1 M KOH at a scanning rate of 50 mV/s at 1600 rpm; (B) Current—time (i—t) chronoamperometric responses for ORR at the Au/rGO hybrids and commercial Pt/C electrodes in an O_2-saturated 0.1 M KOH solution at −0.2 V vs Ag/AgCl.

Au/rGO hybrids may not only serve as the support but also plays a key role in the support—metal interactions.[31,56,57] It has been demonstrated theoretically that, in the noble metal clusters/defective graphene hybrids, the defective graphene substrate may lower the dissociation activation energy of molecular O_2 by accelerating the charge transfer from metal atoms to molecular O_2 and meanwhile decrease the energy barrier of the rate-limiting step by reducing the stability of the intermediate species of ORR.[31]

Finally, the durability of Au/rGO and commercial Pt/C during ORR is evaluated via the chronoamperometric method at −0.20 V vs Ag/AgCl in an O_2-saturated 0.1 M KOH solution. Impressively, the current density at the Au/rGO hybrids shows a much slower decay than that at the Pt/C electrode (Figure 5B). About 16% loss of the current density occurs for the Au/rGO hybrids after 40000 s, while the corresponding current loss at the Pt/C electrode under the same condition is as high as 50%. This result exemplifies that the Au/rGO catalyst is more stable than the commercial Pt/C electrode (Figure 5 and Supporting Information, Figure S10). TEM observation after the durability test also indicates that the Au clusters are stable without noticeable size change and cluster aggregation (Supporting Information, Figure S11). The durability of catalysts is further investigated by the accelerated degradation test (ADT) which is designed to simulate PEM fuel cell working conditions.[63] Supporting Information, Figure S12 shows the RDE curves of Au/rGO hybrids and commercial Pt/C in O_2-saturated 0.1 M KOH at a scanning rate of 50 mV/s at 1600 rpm before and after 20 h ADT. It is observed that the onset potential of Au/rGO has only a 33 mV degradation; in contrast, the corresponding

change for commercial Pt/C is as high as 82 mV. This result also indicates that the Au/rGO catalyst is more stable than the commercial Pt/C, which is consistent with the data evaluated by the chronoamperometric method (Figure 5B). Such a high stability of the Au/rGO hybrids should originate from two aspects: the covalent hybridization between the Au cluster and rGO substrate prevent possible migration and aggregation of Au clusters sintering (as shown in Supporting Information, Figure S11), and the graphitic structure of rGO support intrinsically possesses the high corrosion resistance as compared with other activated carbon support.[64]

CONCLUSION

In summary, a new and general strategy known as the "clean" method has been developed to grow ultrafine Au clusters and other metal clusters (Pt, Pd) on the rGO sheets without any additional protecting molecule or reductant. Different from the previous mechanisms, it is found that the strong absorption capacity of rGO sheets toward metal ions is in favor of providing the initial nuclear sites and restraining growth of Au clusters. In this process, rGO sheets are explored to serve as the electron donors for reducing Au ions. The Au/rGO hybrids exhibit excellent eletrocatalytic performance toward ORR, which has a comparable onset potential to commercial Pt/C catalyst, but superior methanol tolerance and enhanced electrocatalytic stability. This work not only offers a low-cost and high performance alternative for Pt catalysts in fuel cells, but also opens the door toward fabrication of varying types of metal cluster/graphene hybrids that will have wide application in the catalysis, environmental, and new energy fields.

METHODS

Synthesis of Graphene Oxide (GO), Reduced Graphene Oxide (rGO), and Au/rGO. GO was synthesized according to the Hummers' method.[58,59] The rGO sheets in the solution were synthesized following Li's method:[32] 125 mg of GO was dispersed in 500 mL

of water to obtain a 0.025 wt % solution in a 1000-mL three-necked bottle, and then 350 μL of hydrazine solution (25 wt % in water) and 2 mL of ammonia solution (25 wt % in water) were added to the solution. After the mixture was vigorously shaken for a few minutes, 10 mL of isooctane was added to form a

uniform organic layer on top of the aqueous solution. The solution then was incubated in an oil bath (95 °C) for 1 h. Finally, the obtained rGO colloids were set aside for at least two weeks to remove the residual N_2H_4. After reduction, the mass concentration of rGO sheets was about 0.17 mg/mL.

100 μL of 50 mM $HAuCl_4$ aqueous solution was added to 10 mL of rGO sheet solution at room temperature with an initial ultrasonic procedure. After 10 min, the resulting products were collected by centrifugation and washed several times with pure water. The final Au/rGO products were obtained by a freeze-drying method. By XPS analysis, the atoms content of Au in Au/rGO was 1.8 atom %, and the weight content was 22.6 wt %.

Characterizations. TEM was performed on a FEI Tecnai G2 F20 electron microscope operated at 200 kV, and energy-dispersive X-ray spectra (EDX) was performed on Horiba EMAX 7593-H. The surface morphology was examined under a Hitachi S4800 scanning electron microscope. XPS spectra were performed by an ESCALAB 20 Xi XPS system, where the analysis chamber was 1.5×10^{-9} mbar and the size of X-ray spot was 500 μm. Raman spectra were obtained by Renishaw inVia microscope. A He−Ne laser (633 nm) was used as the light source for excitation.

Electrochemical Measurements. *N,N*-Dimethylformamide (DMF) was chosen as the organic solvent to disperse rGO and Au/rGO hybrids because of its proper polarity and relatively lower boiling point. A 2 mg portion of the Au/rGO hybrids was dispersed in 1 mL of DMF by 1 h of ultrasonication to form a Au/rGO catalyst ink. The rGO and Au NP/rGO inks were also prepared by 1 h of ultrasonication in DMF (2 mg/mL). For commercial Pt/C catalyst (20 wt % Pt), 4 mg of Pt/C catalysts were dispersed in 1 mL of ethanol with 35 μL of 5 wt % Nafion solution by 1 h of ultrasonication. The Au cluster catalyst ink was prepared by dissolving 2 mg of as-prepared Au clusters in 1 mL of dichloromethane.

For fabrication of the working electrodes of Au/rGO, Au NP/rGO, and Au clusters, 10 μL of catalyst ink was loaded onto a glass carbon electrode of 5 mm in diameter (loading about 0.1 mg/cm^2), and then a drop of Nafion solution (5 μL, 0.5 wt %) was cast on the electrode. Then the electrode was dried at 60 °C. For fabrication of the working electrode of Pt/C catalyst, 5 μL of catalyst ink was loaded onto a glass carbon electrode of 5 mm in diameter. This electrode was dried at room temperature.

Cyclic voltammetry was performed in a three-electrode electrochemical cell using Pt wire and a Ag/AgCl electrode as counter-electrode and reference electrode, respectively. For all the electrochemical measurements, an aqueous solution of 0.1 M KOH was used as electrolyte. N_2 or O_2 was used to purge the solution to achieve an O_2-free or O_2-saturated condition. All the experiments were carried out at room temperature.

Rotating disk electrode (RDE) measurements were performed using the Koutecky−Levich equation.[60,61] This equation was used to determine the number of electrons involved in oxygen reduction using Au/rGO hybrids. Koutecky−Levich plots (J^{-1} vs $\omega^{-1/2}$) were analyzed at various electrode potentials. The slopes of their best linear fit lines were used to calculate the number of electrons transferred (n) on the basis of the Koutecky−Levich equation:

$$1/J = 1/J_L + 1/J_K = 1/B\omega^{0.5} + 1/J_K$$

where J_K and J_L were the kinetic- and diffusion-limiting current densities, respectively, and ω was the angular velocity. B was Levich slope that was given by

$$B = 0.20nFC_0D_0^{2/3}\nu^{-1/6}; \quad J_K = nFkC_0$$

Here n was the number of electrons transferred in the reduction of one O_2 molecule, F was the Faraday constant (F = 96485 C/mol), D_{O_2} was the diffusion coefficient of O_2 in 0.1 M KOH (D_{O_2} = 1.9×10^{-5} cm^2 s^{-1}), ν was the kinematics viscosity for KOH (ν = 0.01 cm^2 s^{-1}) and C_{O_2} was concentration of O_2 in the solution ($C_{O_2} = 1.2 \times 10^{-6}$ mol cm^{-3}). The constant of 0.2 was adopted when the rotation speed was expressed in rpm.

For rotating ring-disk electrode (RRDE) measurements, a rotating ring disk electrode with a glassy carbon disk (5 mm in diameter) was used (Pine Instruments, model: AFMSRCE). The ring potential was constantly set at 0.5 V vs Ag/AgCl. The electron transfer number (n) was determined by the following equations:[62]

$$n = 4\frac{I_d}{I_d + I_r/N}$$

where I_d was the disk current, I_r was the ring current, and N was the collection efficiency of the ring electrode that was determined to be 0.4 of our electrode.

The accelerated degradation test (ADT) was performed according to ref 63. The RDE curves of Au/rGO and commercial Pt/C were recorded before and after 20 h of ADT testing, respectively.

Conflict of Interest: The authors declare no competing financial interest.

Supporting Information Available: Synthetic procedure of rGO with different reduction state, different types of Au/rGO hybrids, Pd/rGO, Pt/rGO, AuNPs/rGO, and Au clusters. XPS, TEM, UV−vis spectra, and CV data. This material is available free of charge *via* the Internet at http://pubs.acs.org.

REFERENCES AND NOTES

1. Winter, M.; Brodd, R. J. What are Batteries, Fuel Cells, and Supercapacitors. *Chem. Rev.* **2004**, *104*, 4245–4269.
2. Gasteiger, H. A.; Kocha, S. S.; Sompalli, B.; Wagner, F. T. Activity Benchmarks and Requirements for Pt, Pt-Alloy, and Non-Pt Oxygen Reduction Catalysts for PEMFCs. *Appl. Catal. B: Environ.* **2005**, *56*, 9–35.
3. Gewirth, A. A.; Thorum, M. S. Electroreduction of Dioxygen for Fuel-Cell Applications: Materials and Challenges. *Inorg. Chem.* **2010**, *49*, 3557–3566.
4. Debe, M. K. Electrocatalyst Approaches and Challenges for Automotive Fuel Cells. *Nature* **2012**, *486*, 43–51.
5. Gong, K.; Du, F.; Xia, Z.; Durstock, M.; Dai, L. Nitrogen-Doped Carbon Nanotube Arrays with High Electrocatalytic Activity for Oxygen Reduction. *Science* **2009**, *323*, 760–764.
6. Wu, G.; More, K. L.; Johnston, C. M.; Zelenay, P. High-Performance Electrocatalysts for Oxygen Reduction Derived from Polyaniline, Iron, and Cobalt. *Science* **2011**, *332*, 443–447.
7. Suntivich, J.; Gasteiger, H. A.; Yabuuchi, N.; Nakanishi, H.; Goodenough, J. B.; Shao-Horn, Y. Design Principles for Oxygen-Reduction Activity on Perovskite Oxide Catalysts for Fuel Cells and Metal-Air Batteries. *Nat. Chem.* **2011**, *3*, 546–550.
8. Liang, Y.; Li, Y.; Wang, H.; Zhou, J.; Wang, J.; Regier, T.; Dai, H. Co₃O₄ Nanocrystals on Graphene as a Synergistic Catalyst for Oxygen Reduction Reaction. *Nat. Mater.* **2011**, *10*, 780–786.
9. Thorseth, M. A.; Tornow, C. E.; Tse, E. C. M.; Gewirth, A. A. Cu Complexes that Catalyze the Oxygen Reduction Reaction. *Coord. Chem. Rev.* **2012**, dx.doi.org/10.1016/j.ccr.2012.03.033.
10. Nøskov, J. K.; Rossmeisl, J.; Logadottir, A.; Lindqvist, L.; Kitchin, J. R.; Bligaard, T.; Jónsson, H. Origin of the Overpotential for Oxygen Reduction at a Fuel-Cell Cathode. *J. Phys. Chem. B* **2004**, *108*, 17886–17892.
11. According to the definition from Wikipedia, nanoparticles are sized between 1 and 100 nm, while clusters are referred to particles with the dimensions between 1 and 10 nm and a narrow size distribution.
12. Chen, W.; Chen, S. Oxygen Electroreduction Catalyzed by Gold Nanoclusters: Strong Core Size Effects. *Angew. Chem., Int. Ed.* **2009**, *48*, 4386–4389.
13. Jeyabharathi, C.; Kumar, S. S.; Kiruthika, G. V. M; Phani, K. L. N. Aqueous CTAB-Assisted Electrodeposition of Gold Atomic Clusters and Their Oxygen Reduction Electrocatalytic Activity in Acid Solutions. *Angew. Chem., Int. Ed.* **2010**, No.), 2925–2928.
14. Schmid, G.; Chi, L. F. Metal Clusters and Colloids. *Adv. Mater.* **1998**, *10*, 515–526.

15. Häkkinen, H. Atomic and Electronic Structure of Gold Clusters: Understanding Flakes, Cages and Superatoms from Simple Concepts. *Chem. Soc. Rev.* **2008**, *37*, 1847–1859.

16. Lu, Y.; Chen, W. Sub-nanometer Sized Metal Clusters: From Synthetic Challenges to the Unique Property Discoveries. *Chem. Soc. Rev.* **2012**, *41*, 3594–3623.

17. Greeley, J.; Rossmeis, J.; Hellman, A.; Nørskov, J. K. Theoretical Trends in Particle Size Effects for the Oxygen Reduction Reaction. *Z. Phys. Chem.* **2007**, *221*, 1209–1220.

18. Lee, Y.; Loew, A.; Sun, S. Surface- and Structure-Dependent Catalytic Activity of Au Nanoparticles for Oxygen Reduction Reaction. *Chem. Mater.* **2010**, *22*, 755–761.

19. Li, D.; Wang, C.; Tripkovic, D.; Sun, S.; Markovic, N. M.; Stamenkovic, V. R. Surfactant Removal for Colloidal Nanoparticles from Solution Synthesis: The Effect on Catalytic Performance. *ACS Catal.* **2012**, *2*, 1358–1362.

20. Wang, Y. J.; Wilkinson, D. P.; Zhang, J. Noncarbon Support Materials for Polymer Electrolyte Membrane Fuel Cell Electrocatalysts. *Chem. Rev.* **2011**, *111*, 7625–7651.

21. Geim, A. K.; Novoselov, K. S. The Rise of Graphene. *Nat. Mater.* **2007**, *6*, 183–191.

22. Park, S.; Ruoff, R. S. Chemical Methods for the Production of Graphenes. *Nat. Nanotechnol.* **2009**, *4*, 217–224.

23. Allen, M. J.; Tung, V. C.; Kaner, R. B. Honeycomb Carbon: A Review of Graphene. *Chem. Rev.* **2010**, *110*, 132–145.

24. Kamat, P. V. Graphene-Based Nanoarchitectures. Anchoring Semiconductor and Metal Nanoparticles on a Two-Dimensional Carbon Support. *J. Phys. Chem. Lett.* **2010**, *1*, 520–527.

25. Wu, D.; Zhang, F.; Liu, P.; Feng, X. Two-Dimensional Nanocomposites Based on Chemically Modified Graphene. *Chem.—Eur. J.* **2011**, *17*, 10804–10812.

26. Son, D. I.; Kwon, B. W.; Park, D. H.; Seo, W.-S.; Yi, Y.; Angadi, B.; Lee, C.-L.; Choi, W. K. Emissive ZnO−Graphene Quantum Dots for White-Light-Emitting Diodes. *Nat. Nanotechnol.* **2012**, *7*, 465–471.

27. Xu, W.-P.; Zhang, L.-C.; Li, J.-P.; Lu, Y.; Li, H.-H.; Ma, Y.-N.; Wang, W.-D.; Yu, S.-H. Facile Synthesis of Silver@Graphene Oxide Nanocomposites and Their Enhanced Antibacterial Properties. *J. Mater. Chem.* **2011**, *21*, 4593–4597.

28. Cong, H.-P.; Ren, X.-C.; Wang, P.; Yu, S.-H. Macroscopic Multifunctional Graphene-Based Hydrogels and Aerogels by a Metal Ion Induced Self-Assembly Process. *ACS Nano* **2012**, *6*, 2693–2703.

29. Zhou, M.; Zhang, A.; Dai, Z.; Feng, P.; Zhang, C. Strain-Enhanced Stabilization and Catalytic Activity of Metal Nanoclusters on Graphene. *J. Phys. Chem. C* **2010**, *114*, 16541–16546.

30. Lim, D.-H.; Wilcox, J. DFT-Based Study on Oxygen Adsorption on Defective Graphene-Supported Pt Nanoparticles. *J. Phys. Chem. C* **2011**, *115*, 22742–22747.

31. Lim, D.-H.; Wilcox, J. Mechanisms of the Oxygen Reduction Reaction on Defective Graphene-Supported Pt Nanoparticles from First-Principles. *J. Phys. Chem. C* **2012**, *116*, 3653–3660.

32. Li, D.; Muller, M. B.; Gilje, S.; Kaner, R. B.; Wallace, G. B. Processable Aqueous Dispersions of Graphene Nanosheets. *Nat. Nanotechnol.* **2008**, *3*, 101–105.

33. Subrahmanyam, K. S.; Manna, A. K.; Pati, S. K.; Rao, C. N. R. A Study of Graphene Decorated with Metal Nanoparticles. *Chem. Phys. Lett.* **2010**, *497*, 70–75.

34. Wertheim, G. M.; DiCenzo, S. B.; Youngquist, S. E. Unit Charge on Supported Gold Clusters in Photoemission Final State. *Phys. Rev. Lett.* **1983**, *51*, 2310–2313.

35. Turner, M.; Golovko, V. B.; Vaughan, O. P. H.; Abdulkin, P.; Murcia, A. B.; Tikhov, M. S.; Johnson, B. F. G.; Lambert, R. M. Selective Oxidation with Dioxygen by Gold Nanoparticle Catalysts Derived from 55-Atom Clusters. *Nature* **2008**, *454*, 981–983.

36. Chen, X.; Wu, G.; Chen, J.; Chen, X.; Xie, Z.; Wang, X. Synthesis of "Clean" and Well-Dispersive Pd Nanoparticles with Excellent Electrocatalytic Property on Graphene Oxide. *J. Am. Chem. Soc.* **2011**, *133*, 3693–3695.

37. Koo, H. Y.; Lee, H.-J.; Noh, Y.-Y.; Lee, E.-S.; Kim, Y.-H.; Choi, W.-S. Gold Nanoparticle-Doped Graphene Nanosheets: Sub-nanosized Gold Clusters Nucleate and Grow at the Nitrogen-Induced Defects on Graphene Surfaces. *J. Mater. Chem.* **2012**, *22*, 7130–7135.

38. Stankovich, S.; Dikin, D. A.; Piner, R. D.; Kohlhaas, K. A.; Kleinhammes, A.; Jia, Y.; Wu, Y.; Nguyen, S. T.; Ruoff, R. S. Synthesis of Graphene-Based Nanosheets *via* Chemical Reduction of Exfoliated Graphite Oxide. *Carbon* **2007**, *45*, 1558–1565.

39. Gómez-Navarro, C.; Meyer, J. C.; Sundaram, R. S.; Chuvilin, A.; Kurasch, S.; Burghard, M.; Kern, K.; Kaiser, U. Atomic Structure of Reduced Graphene Oxide. *Nano Lett.* **2010**, *10*, 1144–1148.

40. Quintana, M.; Spyrou, K.; Grzelczak, M.; Browne, W. R.; Rudolf, P.; Prato, M. Functionalization of Graphene *via* 1, 3-Dipolar Cycloaddition. *ACS Nano* **2010**, *4*, 3527–3533.

41. Jia, Y. F.; Xiao, B.; Thomas, K. M. Adsorption of Metal Ions on Nitrogen Surface Functional Groups in Activated Carbons. *Langmuir* **2002**, *18*, 470–478.

42. Wagner, A. J.; Wolfe, G. M.; Fairbrother, D. H. Reactivity of Vapor-Deposited Metal Atoms with Nitrogen-Containing Polymers and Organic Surfaces Studied by *in situ* XPS. *Appl. Surf. Sci.* **2003**, *219*, 317–328.

43. Wu, J.-B.; Lin, Y.-F.; Wang, J.; Chang, P.-J.; Tasi, C.-P.; Lu, C.-C.; Chiu, H.-T.; Yang, Y.-W. Correlation between N 1s XPS Binding Energy and Bond Distance in Metal Amido, Imido, and Nitrido Complexes. *Inorg. Chem.* **2003**, *42*, 4516–4518.

44. Ji, X.; Song, X.; Li, J.; Bai, Y.; Yang, W.; Peng, X. Size Control of Gold Nanocrystals in Citrate Reduction: The Third Role of Citrate. *J. Am. Chem. Soc.* **2007**, *129*, 13939–13948.

45. Huo, Z.; Tsung, C.; Huang, W.; Zhang, X.; Yang, P. Sub-Two Nanometer Single Crystal Au Nanowires. *Nano Lett.* **2008**, *8*, 2041–2044.

46. Choi, H. C.; Shim, M.; Bangsaruntip, S.; Dai, H. Spontaneous Reduction of Metal Ions on the Sidewalls of Carbon Nanotubes. *J. Am. Chem. Soc.* **2002**, *124*, 9058–9059.

47. Gentry, S. T.; Fredericks, S. J.; Krchnavek, R. Controlled Particle Growth of Silver Sols through the Use of Hydroquinone as a Selective Reducing Agent. *Langmuir* **2009**, *25*, 2613–2621.

48. Yang, J.; Yin, H.; Jia, J.; Wei, Y. Facile Synthesis of High-Concentration, Stable Aqueous Dispersions of Uniform Silver Nanoparticles Using Aniline as a Reductant. *Langmuir* **2011**, *27*, 5047–5053.

49. Bard, A. J.; Faulkner, L. R. *Electrochemical Methods. Fundamentals and Applications*, 2nd ed.; John Wiley and Sons, Inc.: New York, 2001; Appendix C.

50. Erikson, H.; Jürmann, G.; Sarapuu, A.; Potter, R. J.; Tammeveski, K. Electroreduction of Oxygen on Carbon-Supported Gold Catalysts. *Electrochim. Acta* **2009**, *54*, 7483–7489.

51. Jirkovský, J. S.; Halasa, M.; Schiffrin, D. J. Kinetics of Electrocatalytic Reduction of Oxygen and Hydrogen Peroxide on Dispersed Gold Nanoparticles. *Phys. Chem. Chem. Phys.* **2010**, *12*, 8042–8052.

52. Hu, Y.; Jin, J.; Wu, P.; Zhang, H.; Cai, C. Graphene−Gold Nanostructure Composites Fabricated by Electrodeposition and Their Electrocatalytic Activity Toward the Oxygen Reduction and Glucose Oxidation. *Electrochim. Acta* **2010**, *56*, 491–500.

53. Tang, W.; Lin, H.; Kleiman-Shwarsctein, A.; Stucky, G. D.; McFarland, E. W. Size-Dependent Activity of Gold Nanoparticles for Oxygen Electroreduction in Alkaline Electrolyte. *J. Phys. Chem. C* **2008**, *112*, 10515–10519.

54. Pal, R.; Wang, L.; Pei, Y.; Wang, L.; Zeng, X. C. Unraveling the Mechanisms of O_2 Activation by Size-Selected Gold Clusters: Transition from Superoxo to Peroxo Chemisorption. *J. Am. Chem. Soc.* **2012**, *134*, 9438–9445.

55. Chen, W.; Ny, D.; Chen, S. SnO_2−Au Hybrid Nanoparticles as Effective Catalysts for Oxygen Electroreduction in Alkaline Media. *J. Power Sources* **2010**, *195*, 412–418.

56. Slanac, D. A.; Lie, A.; Paulson, J. A.; Stevenson, K. J.; Johnston, K. P. Bifunctional Catalysts for Alkaline Oxygen Reduction Reaction *via* Promotion of Ligand and Ensemble Effects at Ag/MnO_x Nanodomains. *J. Phys. Chem. C* **2012**, *116*, 11032–11039.

57. Slanac, D. A.; Hardin, W. G.; Johnston, K. P.; Stevenson, K. J. Atomic Ensemble and Electronic Effects in Ag-Rich AgPd Nanoalloy Catalysts for Oxygen Reduction in Alkaline Media. *J. Am. Chem. Soc.* **2012**, *134*, 9812–9819.

58. Hummers, W. S.; Offeman, R. E. Preparation of Graphitic Oxide. *J. Am. Chem. Soc.* **1958**, *70*, 1339–1339.

59. Titelman, G. I.; Gelman, V.; Bron, S.; Khalfin, R. L.; Cohen, Y.; Bianco-Peled, H. Characteristics and Microstructure of Aqueous Colloidal Dispersions of Graphite Oxide. *Carbon* **2005**, *43*, 641–649.

60. Qu, L. T.; Liu, Y.; Baek, B. J.; Dai, L. M. Nitrogen-Doped Graphene as Efficient Metal-Free Electrocatalyst for Oxygen Reduction in Fuel Cells. *ACS Nano* **2010**, *4*, 1321–1326.

61. Li, Y.; Zhao, Y.; Cheng, H.; Hu, Y.; Shi, G.; Dai, L.; Qu, L. Nitrogen-Doped Graphene Quantum Dots with Oxygen-Rich Functional Groups. *J. Am. Chem. Soc.* **2012**, *134*, 15–18.

62. Liang, Y.; Wang, H.; Zhou, J.; Li, Y.; Wang, J.; Regier, T.; Dai, H. Covalent Hybrid of Spinel Manganese–Cobalt Oxide and Graphene as Advanced Oxygen Reduction Electrocatalysts. *J. Am. Chem. Soc.* **2012**, *134*, 3517–3523.

63. Shao, Y.; Kou, R.; Wang, J.; Viswanathan, V. V.; Kwak, J. H.; Liu, J.; Wang, Y.; Lin, Y. The Influence of the Electrochemical Stressing (Potential Step and Potential-Static Holding) on the Degradation of Polymer Electrolyte Membrane Fuel Cell Electrocatalysts. *J. Power Sources* **2008**, *185*, 280–286.

64. Shao, Y.; Zhang, S.; Wang, C.; Nie, Z.; Liu, J.; Wang, Y.; Lin, Y. Highly Durable Graphene Nanoplatelets Supported Pt Nanocatalysts for Oxygen Reduction. *J. Power Sources* **2010**, *195*, 4600–4605.